Korean J. Chem. Eng., 33(1), 319-329 (2016)
DOI: 10.1007/s11814-015-0102-2

pISSN: 0256-1115
eISSN: 1975-7220

Synthesis and characterization of polyhedral oligomeric silsesquioxane-based waterborne polyurethane nanocomposites

Hengameh Honarkar*, Mohammad Barmar*,†, Mehdi Barikani*, and Parvin Shokrollahi**

*Polyurethane and Advanced Polymers Department, Faculty of Science, Iran Polymer and Petrochemical Institute, Tehran, Iran
**Biocompatible Polymers Department, Faculty of Science, Iran Polymer and Petrochemical Institute, Tehran, Iran
(*Received 14 February 2015 • accepted 14 May 2015*)

Abstract−A series of aqueous polyurethane nanocomposites were prepared using various amounts (0.3-4.6 wt%) of a diol functionalized polyhedral oligomeric silsesquioxane (POSS) by the prepolymer mixing method. *N,N*-bis(2-hydroxy ethyl-2-amino ethane sulfonic acid sodium salt (BES sodium salt) was used as the anionic internal emulsifier and ionic center. The molecular structure of the samples was characterized by ATR-FTIR spectroscopy. We investigated the effect of the POSS contents on the properties of the specimens by particle size and viscosity measurements, X-ray diffractometry, mechanical behavior assessment, dynamic mechanical thermal analysis (DMTA), thermogravimetric analysis and morphological studies. The results showed that with increasing the POSS contents, particle size, viscosity, tensile strength, modulus, T_g, and thermal stability of the synthesized samples were improved. Also, SEM and TEM images indicated that a homogeneous morphology was obtained in the 1.2 wt% POSS-based sample. AFM results showed that the surface roughness increased as the POSS amounts increased.

Keywords: Nanocomposites, Aqueous Polyurethane, POSS, Anionic, Emulsifier

INTRODUCTION

There has been growing interest in organic-inorganic hybrid polymers. By incorporation of the inorganic moieties into the chains of organic polymers, it is possible to obtain polymer hybrids. Reactive polyhedral oligomeric silsesquioxanes (POSS) are functional nanoscale fillers with formula of $(RSiO_{1.5})_8$ - based cage containing eight corners bearing one or more functional groups applied for this purpose, where R can be hydrogen, vinyl, alkyl, aryl, epoxy or their derivatives [1-5]. The POSS cages are known as an organic-inorganic hybrid with a size of approximately 1 to 3 nm. POSS can be incorporated by three procedures into a polymer matrix to afford nanocomposites: (1) mechanical melt blending as typical nanofiller, (2) covalent chemical bonds formation via reaction of functional groups on the POSS cage corners, and (3) reacting POSS macromer possessing a single polymerizable functional group with a suitable monomer. In the first procedure, all eight corners of the cage structure of POSS are substituted by unreactive R groups. In the second route, based on the number of functional groups, POSS molecules can be incorporated into the polymer structure as a node of the polymer network and a part of the main backbone or side chains. Also, variation in the nature or the size of the outer functional group, results in the production of various numbers of POSS-based molecules with a wide range of chemical and physical properties. In the third method the macromer is copolymerized with a suitable monomer, yielding a desired organic-inorganic hybrid [6].

Recently, novel hybrid systems based on poly (styrene-b-(ethylene-co-butylene)-b-styrene) (SEBS) and POSS have been synthesized by click chemistry. These nanohybrid materials show excellent mechanical properties and thermal stability. It is due to both the homogeneous dispersion and compatibility of POSS molecules with polymer matrix and the covalent bond formation between SEBS and POSS molecules [7].

POSS has been applied to study and improve the characteristic behavior of different materials such as polypropylene [8], polystyrene [9], cellulose acetate [10], polyamide [11], cotton/polyester fabric [12], polyimide [13], and epoxy [14]. Another usage of POSS is plasticization of poly (vinyl chloride) [15]. Also, the application of toughened poly (methyl methacrylate)-POSS nanocomposite [16], POSS/polycarbonate [17], and poly (ethylene oxide)-functionalized POSS as electrolyte in lithium batteries has been reported [18].

Wang et al. synthesized novel polymethacrylate [19] and polycarboxyl [20] functionalized POSS networks. These materials are utilized as nanofiller and cross-linker to copolymerize with methyl methacrylate and to cure diglycidyl ether of bisphenol-A (DGEBA), respectively. In this way they obtained inorganic/organic polymer nanocomposites with desired properties.

Also, Zhou et al. prepared PBT/POSS composites via melting blending with small quantities of POSS [21]. The incorporation of the POSS molecules results in reduced flammability [22,23], enhanced mechanical properties and thermal stability [24], and production of resistant materials [25].

In recent years, many investigations have been conducted on polyurethanes [26,27] and polyurethane/POSS systems [28-33]. The reaction of the functionalized POSS with polyurethane ingredients has been achieved via the melt processing or in solution. Regarding ecosystem considerations, the attention is focused on the prepara-

†To whom correspondence should be addressed.
E-mail: m.barmar@ippi.ac.ir
Copyright by The Korean Institute of Chemical Engineers.

tion of aqueous polyurethane dispersions using minimum level of organic solvents [34-36]. The waterborne polyurethane dispersion is a binary colloidal system in which the particles of polyurethane are dispersed in the continuous aqueous medium. Polyurethane is completely incompatible with water, so a special modification on the backbone is necessary. This concept is achievable by the incorporation of hydrophilic monomers or monomers containing ionic functionality such as quaternary ammonium, carboxylate or sulfonate groups. These ionic moieties are known as internal emulsifiers. Nanda and coworkers synthesized an aqueous POSS/polyurethane-urea nanocomposite by the acetone process in which dimethylol propionic acid (DMPA) and triethyl amine (TEA) were used as ionic center and neutralizer, respectively. The results showed that POSS was homogeneously incorporated into the polyurethane hard segments and physical properties such as modulus, complex viscosity and surface hydrophobicity had changed significantly [37].

Note that very few investigations have been reported in the field of waterborne polyurethane-POSS nanocomposites and this new class of hybrid polyurethane is suitable for coating applications [38,39].

Sulfonated polyurethane dispersions show an excellent hydrolytic stability over a wide range of pH values. Therefore, to obtain a stable polyurethane dispersion, sulfonate groups are preferred due to increased hydrophilicity and stabilization efficiency [40].

We synthesized a series of waterborne polyurethane nanocomposites using different values (0.3-4.6 wt%) of a diol functionalized polyhedral oligomeric silsesquioxane (1,2-propanediol isobutyl POSS). The samples were prepared using *N,N*-bis(2-hydroxyethyl)-2-amino ethane sulfonic acid sodium salt (BES sodium salt) as sulfonated ionic center, poly(ε-caprolactone, PCL), hydrogenated MDI (H_{12}MDI), and 1,4 butanediol (BDO). The prepolymer mixing method was employed for synthesis of compounds. Incorporation of BES sodium salt ionic center has not been studied in any system, and the properties that impart to waterborne polyurethane nanocomposites have not been investigated before. Furthermore, in the present synthesis, neutralization step is not necessary. A detailed view of the individual reactions will be presented in the next sections.

EXPERIMENTAL

1. Materials

Poly(ε-caprolactone, PCL) with a molecular weight of 2,000 g/mol from Solvay Chemicals (UK), 4,4′-dicyclohexyl methane diisocyanate (H_{12}MDI), (mixture of isomers, 90%), and *N,N*-bis(2-hydroxyethyl)-2-amino ethane sulfonic acid sodium salt (BES sodium salt) from Sigma Aldrich, 1,2-propanediol isobutyl POSS, from Hybrid Plastics (USA), and 1,4 butanediol (BDO) from Merck were utilized in this study. PCL and 1,4 BDO were dried overnight under a static vacuum before use at 60 °C. Also, BES and POSS were dried by a similar procedure at 80 °C. Dibutyltin dilaurate (DBTDL) (Merck) was applied as a catalyst without further purification. H_{12}MDI was used as received. DMSO and Acetone, 98%, both from Merck were used as solvents (after distillation).

2. Characterization

Infrared spectra were recorded on an FTIR (Bruker Equinox 55, Germany) equipped with Golden Gate single reflection ATR-FTIR attachment (attenuated total reflection) accessory. The samples were in the form of polymeric sheets and scanned over the range of 400-4,000 cm^{-1} with a resolution of 4 cm^{-1} at the room temperature.

Particle size was measured by dynamic light scattering (SemaTech, SEM-633, He-Ne laser, France) at room temperature. The samples were homogenized after dilution in deionized water (0.5%). The test was followed by the pinhole being set at 100 μm, angle 90° and experiment duration of 120 s and refractive index of 1.33.

Solution viscosity was measured at 25 °C with a Brookfield viscometer (DV-II+Pro, UL Adapter spindle) at a shear rate of 100 s^{-1}.

The intrinsic viscosity was measured by an Ubbelohde suspended-level viscometer using the flowing time of a dilute solution through a simple glass capillary. The viscosity measurements were made in dimethylformamide (DMF), as solvent at 40 °C±0.01 according to Mark-Houwink equation ($[\eta]=KM^{\alpha}$). Four different samples of dilute polymer solutions were prepared with concentrations between 0.5-2.0 g/dL. Flowing time of the pure solvent (t_0) and the polymer solution (t) were measured. With plotting η_{sp}/c versus c and extrapolation to zero concentration, the intrinsic viscosity was obtained, where, $t/t_0=\eta/\eta_0$ and the specific viscosity was defined as $\eta_{sp}=(\eta/\eta_0)-1$.

X-ray diffraction was applied to study the crystalline and amorphous structure of the synthesized samples. It was carried out by XRD instrument (Siemens, D 5000, Germany) equipped with an FK 60-04 air insulated X-ray diffraction tube with Fe anode. The XRD spectra were obtained using Fe K_{α} radiation (1.936 Å) at 900 W, 35 kV and 25 mA. Also, the scanning was performed in the diffraction angle (2θ) range from 5 to 40° at a rate of 1.2°/min.

Tensile properties of the emulsion cast films were measured at room temperature by using a Santam Universal Testing Machine (STM-20), according to ASTM D638 type V at a crosshead speed of 10 mm/min. In these tests, an average of at least five measurements was taken and a 200 N load cell was used.

Dynamic mechanical thermal analysis (DMTA) was on a Triton (Tritec 2000 DMA, UK) instrument at deformation tensile mode, a frequency of 1 HZ and a heating rate of 5 °C/min from −100 °C to 100 °C with rectangular samples (10×8×1 mm^3).

The thermal stability of the samples was studied with a thermogravimetric analyzer (Mettler Toledo, TGA/DSC1, Switzerland) at a heating rate of 10 °C/min in a nitrogen atmosphere from room temperature to 700 °C. The sample weight was 14 mg in all measurements.

Morphological analyses of the nanocomposites were performed using SEM, TEM and AFM. Cross-sectional morphologies of the samples were examined by SEM using a VEGA SEM\TESCAN electron microscope (Czech Republic). The samples were fractured in liquid nitrogen and fixed on an aluminum stand. Then, a thin layer of Au was sputtered on the surface of them prior to SEM microscopy. An accelerating voltage of 20 kV was used for the SEM measurements.

Microphase separated morphology of the samples was accurately evaluated by TEM analysis. TEM images were obtained by using a Philips (EM 208S, England) transmission electron microscope at 120 kV. The samples were frozen at −100 °C and then, ultrathin layer (20 nm) slices were made using cryo ultramicrotomy (Leica,

EM UC7, Germany) and a diamond knife.

Investigation of the surface topography and roughness was performed with a Dual Scope, non-contact mode atomic force microscope (AFM, 95-200E, DME, Denmark) with a 10 nm radius silicon probe. Surface roughness of the synthesized samples was calculated by DME- SPM software.

3. Synthesis of the Polymer

A 250 mL round-bottom, four-necked flask equipped with a mechanical stirrer with condenser connector, thermometer, nitrogen inlet, and pipette outlet was used as a reactor. The reaction was performed in a constant temperature oil bath. At first, the dried PCL was charged into the dried flask. While stirring, the system was

Table 1. Feed compositions of the synthesized waterborne polyurethane nanocomposites

Sample code	Capa (g)	$H_{12}MDI$ (g)	BES (g)	POSS (wt%)	BDO (g)
N_0	20	7.99	3.53	0.0	0.450
N_1	20	7.99	3.53	0.3	0.441
N_2	20	7.99	3.53	0.6	0.432
N_3	20	7.99	3.53	1.2	0.414
N_4	20	7.99	3.53	2.4	0.378
N_5	20	7.99	3.53	3.5	0.342
N_6	20	7.99	3.53	4.6	0.306

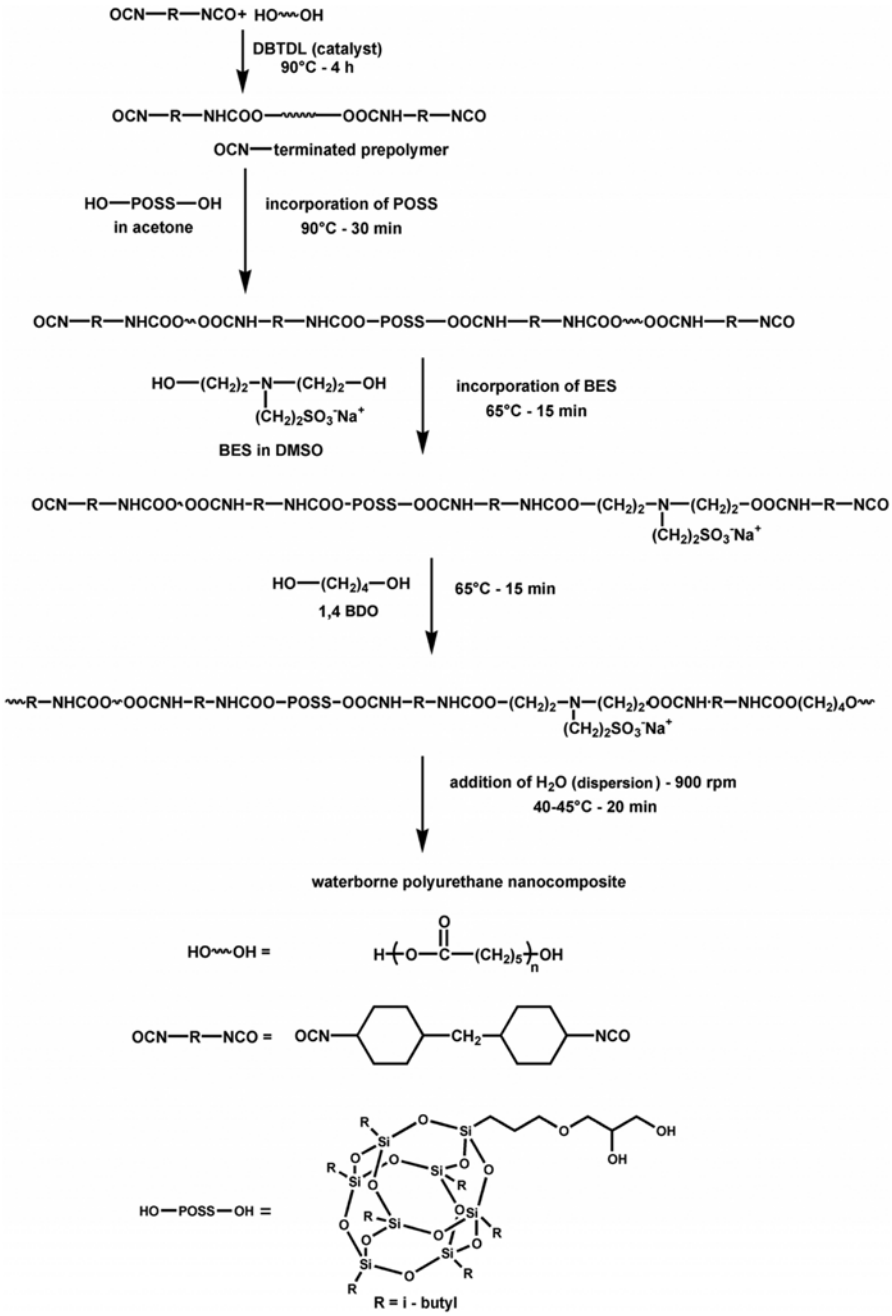

Scheme 1. Schematic illustration of synthesis of the waterborne polyurethane nanocomposites.

heated to 90 °C. Then, H_{12}MDI and the catalyst (two droplets) were added slowly into the reactor with a dropping funnel. In the formulation of the reaction, a stoichiometric excess of diisocyanate was used. So, the NCO-terminated prepolymer was prepared after heating the reaction mixture for 4h at 90 °C. Then, the solution of POSS in acetone was added into the reaction mixture. It was done following reaching the theoretical NCO value. After 30 minutes (this time varied based on POSS amount) the temperature was lowered to 65 °C. The solution of BES in DMSO (minimum amount) was poured into the reactor and stirring was carried on for 15 min. In the next step, butanediol was added at the same temperature and the reaction was continued for a further 15 min. After that, the reactor was cooled to 40-45 °C, and water was introduced dropwise into the reactor at a stirring rate of 900 rpm for 20 min. An appropriate amount of water was added to obtain dispersions with 30 wt% solid content. Then, the obtained aqueous dispersions of the polyurethane nanocomposites were cast onto a Teflon plate at room temperature. After three days, the mold was put in an oven at 100 °C for 8 h. After demolding, the obtained films were stored in a desiccator prior to further characterization. A number of samples were prepared using different percentages of POSS nanoparticles. These synthesized emulsions exhibited very good stability. The compositions and their amounts are shown in Table 1. Also, the reaction scheme including the prepolymer synthesis and processes of chain extension and dispersion are shown in Scheme 1.

RESULTS AND DISCUSSIONS

1. IR Spectroscopy

IR spectroscopy of the samples containing various amounts of POSS was performed after centrifugation of the emulsions to ensure the removal of any probable unreacted POSS macromer. On this basis, IR spectra of the neat POSS-diol and a typical waterborne polyurethane nanocomposite based on 1.2 wt% POSS are shown in Fig. 1. The characteristic absorption peaks in POSS spectrum are 3,436, 2,956, and 2,873 cm^{-1}, which are due to O-H stretching, alkane -CH asymmetric and symmetric stretching vibration of CH_2 groups, respectively. Absorptions at 1,465 and 1,332 cm^{-1} are due to CH_2 and OH bending, respectively. The peak at 1,107 cm^{-1} is attributed to Si-O-Si stretching vibration. Also, the characteristic peaks at 838 and 1,232 cm^{-1} are due to Si-C bending vibration. In the typical polyurethane nanocomposite spectrum based on POSS (for example 1.2 wt% POSS), the characteristic absorption peaks are 2,927 and 2,862 cm^{-1} which are due to alkane -CH asymmetric and symmetric stretching vibration of CH_2 groups. Absorption at 1,529 cm^{-1} is due to CHN vibration of the associated secondary urethane groups (-NH bending). Also, related peaks of CH_2 and CH_3 deformation vibration and C-N stretching are appeared at 1,457 and 1,362 cm^{-1}, respectively.

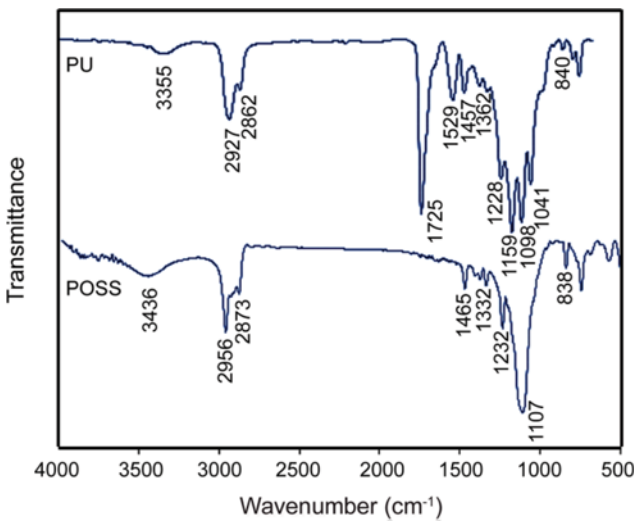

Fig. 1. IR spectra of POSS-diol and PU nanocomposite based on 1.2 wt% POSS.

The C-O-C stretching vibration corresponds to the ether oxygen of the soft segment at 1,041-1,228 cm^{-1}. Note that the above peaks and the mentioned peaks in the POSS spectrum overlap at some regions. Also, the absorption peak at 840 cm^{-1} is due to Si-C vibration and shows the incorporation of POSS in the PU structure. The FTIR spectrum of the mentioned polyurethane nanocomposite shows the characteristic bands of urethane NH groups at 3,355 cm^{-1} (NH stretching) and 1,725 cm^{-1} due to carbonyl (C=O) stretching of urethane and ester groups, which can be considered as an evidence of the PU formation. In this spectrum, the isocyanate absorption peak (-NCO, 2,270 cm^{-1}) disappeared, indicating the -NCO groups completely reacted during the chain extension step [41].

2. Effect of the POSS Contents on Particle Size, Viscosity and Molecular Weight

The effect of the POSS contents on particle size and viscosity of the synthesized emulsions is summarized in Table 2. In the synthesized emulsions, the particle size and viscosity increase with POSS content. When the ionic center was kept constant, the waterborne polyurethane nanocomposite with higher POSS content had a higher average particle size. In fact, at a fixed value of the ionic center in the formulation, the molecular weight of the mixture (before dispersion in water) increased with POSS contents. Therefore, the viscosity of the compound with higher molecular weight is high. Thus, in the step of dispersion, the more viscous mixture including higher POSS content is more hardly to be dispersed in water, and as a result, the dispersion is carried out with larger particle size. A similar conclusion was suggested by Lee et al. using sulfonated polyol to prepare aqueous polyurethane dispersions [42].

Gel permeation chromatography (GPC) could not be used as a

Table 2. Particle size and viscosity of the synthesized waterborne polyurethane nanocomposites

Sample code	POSS (wt%)	Particle size (nm)	η (mPa·s)
N_0	0.0	62.5	18.5
N_1	0.3	62.4	19.1
N_2	0.6	80.9	20.5
N_3	1.2	84.1	24.3
N_4	2.4	97.2	35.5
N_5	3.5	138.3	57.4
N_6	4.6	231.4	74.3

Table 3. Intrinsic viscosity of the synthesized samples in DMF at 40 °C

Sample code	POSS (wt%)	[η] (dL/g)
N_0	0.0	0.39
N_1	0.3	0.41
N_2	0.6	0.45
N_3	1.2	0.49
N_4	2.4	0.53
N_5	3.5	0.59
N_6	4.6	0.64

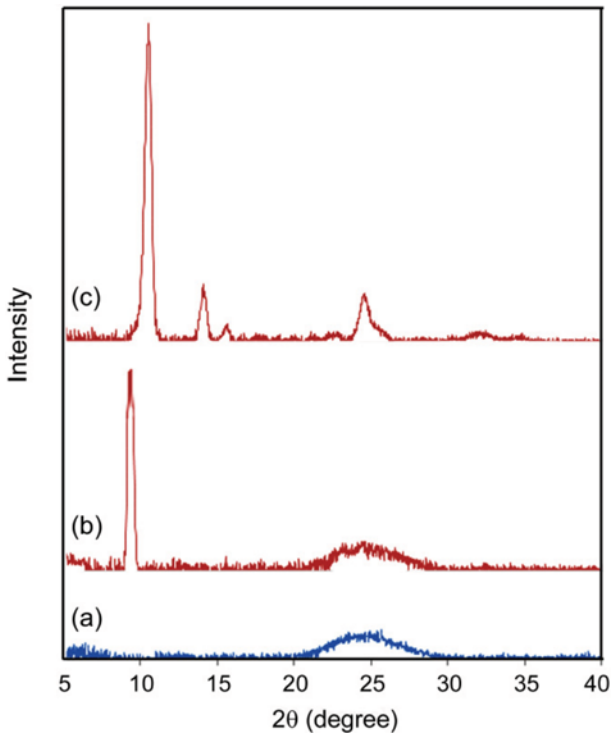

Fig. 2. X-ray diffractions of (a) the neat PU, (b) PU nanocomposite with 1.2 wt% POSS, and (c) the neat POSS.

certain measurement of molecular weight, because the prepared samples were only partially soluble in THF. Therefore, the intrinsic viscosity [η] was measured to obtain information on the molecular weight of the synthesized polyurethanes [43]. In this way, samples containing different amounts of POSS (0-4.6 wt%) were analyzed

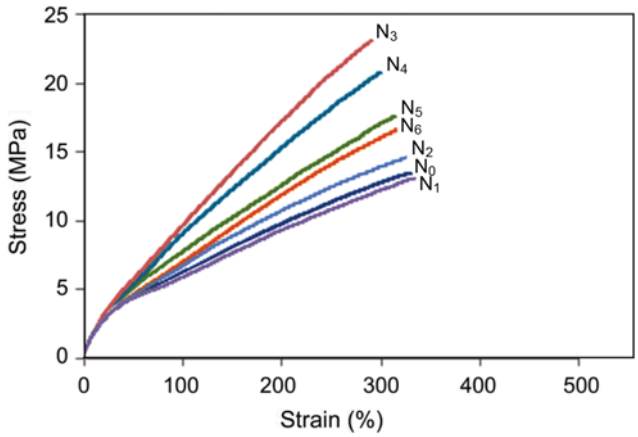

Fig. 3. Stress-strain curves for nanocomposites with different amounts of POSS: N_0 (0.0 wt%), N_1 (0.3 wt%), N_2 (0.6 wt%), N_3 (1.2 wt%), N_4 (2.4 wt%), N_5 (3.5 wt%) and N_6 (4.6 wt%).

by a Ubbelohde capillary viscometer. The results are shown in Table 3. These results are very important to estimate the viscosity average molecular weight (M_v) according to Mark-Houwink equation ([η]=KM^{α}). As can be seen from Table 3, with increasing of the POSS contents, intrinsic viscosity and thereby, molecular weight increase.

3. X-ray Analysis

Fig. 2 shows the wide angle X-ray analysis of the In Fig. 2, in the control sample (N_0), a broad peak at 2θ range of 20-30 is observed which is due to the amorphous phase in the polymer matrix mainly composed of soft segments. The X-ray pattern of the unreacted POSS macromer showed well defined sharp reflections at 2θ=10.33, 13.91, 15.46 and 24.32. In the sample containing 1.2 wt% POSS, there are two peaks at 2θ=9.36 and 24.44. The sharp reflection at 9.36 indicates the presence of the crystalline structure of POSS, which is an evidence for incorporation of POSS into the polyurethane hard segments. Also, the broad peak at 2θ=24.44 is due to the polyurethane matrix. This means that the cages of POSS maintain a self assembling ability when they are incorporated into the hard segments of polyurethane, resulting in formation of a nanocrystalline phase [44].

4. Mechanical Properties

Mechanical properties of the samples with respect to POSS contents are summarized in Table 4.

Fig. 3 shows the stress-strain curves of the emulsion cast films based on the different amounts of POSS. As can be seen in Fig. 3,

Table 4. Mechanical properties of the synthesized waterborne polyurethane nanocomposites

Sample code	POSS content (wt%)	Modulus (MPa)	Tensile strength (MPa)	Elongation-at-break (%)
N_0	0.0	17.13±0.32	13.77±0.37	330±10.4
N_1	0.3	18.97±0.91	13.11±0.11	334±13.7
N_2	0.6	19.43±0.72	14.75±0.17	325±12.5
N_3	1.2	28.50±0.11	23.10±0.18	290±11.3
N_4	2.4	22.97±0.76	20.84±0.21	300±13.8
N_5	3.5	21.23±0.32	17.73±0.19	313±14.6
N_6	4.6	20.46±0.25	16.57±0.16	315±15.3

with increasing the POSS content to 1.2 wt%, the tensile strength increased. But, with incremental increase of the POSS values from 2.4 to 4.6 wt%, the tensile strength decreased. This behavior is explained regarding to the interchain interactions. The interchain attractive forces between hard segments are due to the high concentration of polar groups and the possibility of extensive hydrogen bonding. These forces are much stronger than those present in the soft segments [45]. Hard segments significantly affect mechanical properties, particularly modulus, hardness, and tensile strength. As mentioned earlier, POSS was used as a partial of chain extender and consequently hard segments, thereby the bulky nature of the POSS cages may disrupt the cohesive interchain interactions and therefore cause the mechanical properties to decrease. In some cases, the incorporation of the POSS macromer into the polymer matrix may not improve the mechanical properties [46].

In the present study, the maximum tensile strength is recorded for sample N_3 with 1.2 wt% POSS content. The increase of the POSS concentration results in a higher tensile strength and concurrently lower elongation at break. It is mainly due to dispersion of the POSS macromers within the hard segments of polyurethane that, consequently, the stiffness of the polymer matrix increases.

5. DMTA Studies

The dynamic mechanical properties (storage modulus and tan δ) of the emulsion cast films based on POSS contents are shown in Figs. 4 and 5, respectively. In Fig. 4 the storage modulus increases with increasing the POSS amounts. POSS contributes to the hard segment domains of the PU films and, as a matter of fact, the hard segments improve the mechanical properties such as storage modulus. Therefore, E′ increases with increasing POSS. This occurs up to 1.2 wt% POSS, and after this value modulus slightly decreases. As mentioned earlier, this is due to the bulky structure of the POSS cage which caused the reduction of cohesive interactions and packing of the chains. On the other hand, the glass transition temperature (T_g) of the PU (tan δ) (Fig. 5) moved toward higher temperatures as the POSS content was increased. The POSS macromers are dispersed into the polymer matrix at the molecular level. Compared with traditional fillers, POSS is known in some cases to exhibit enhanced compatibility resulting from a match between its organic substituents and the polymer matrix.[17] Therefore, the POSS molecules can play a role as a compatibilizer between the hard and soft segments and improve the miscibility between the two phases. That is, the POSS molecules act as a diluent and weaken the interactions between the hard segments, allowing them to be dispersed easily within in the soft segments matrix [44,47]. The curves of tan δ for the synthesized samples show a rising T_g of the soft segment up to 10 °C (from T_g of N_0: −35.83 to T_g of N_6: −25.5 °C) with increasing of the POSS amounts. An increase in T_g of the soft segment

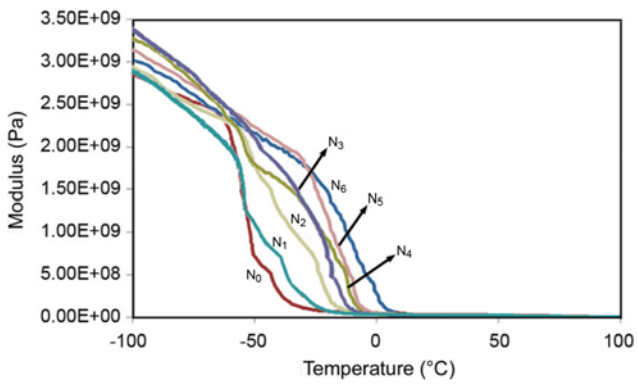

Fig. 4. Storage modulus of the samples containing different amounts of POSS: N_0 (0.0 wt%), N_1 (0.3 wt%), N_2 (0.6 wt%), N_3 (1.2 wt%), N_4 (2.4 wt%), N_5 (3.5 wt%) and N_6 (4.6 wt%).

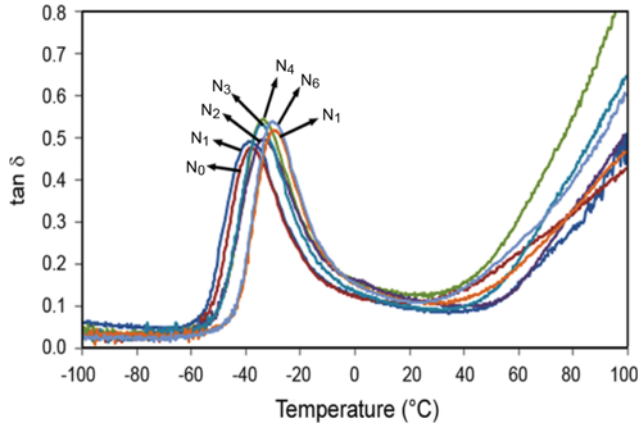

Fig. 5. Variations of tan δ for the samples based on different amounts of POSS: N_0 (0.0 wt%), N_1 (0.3 wt%), N_2 (0.6 wt%), N_3 (1.2 wt%), N_4 (2.4 wt%), N_5 (3.5 wt%) and N_6 (4.6 wt%).

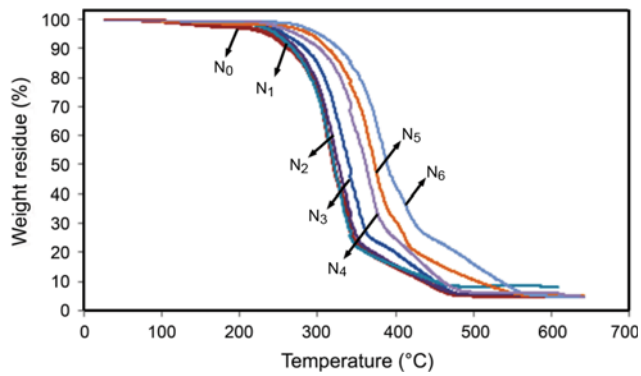

Fig. 6. Thermal stability of the samples as a function of the POSS content: N_0 (0.0 wt%), N_1 (0.3 wt%), N_2 (0.6 wt%), N_3 (1.2 wt%), N_4 (2.4 wt%), N_5 (3.5 wt%) and N_6 (4.6 wt%).

Table 5. Thermal behavior of the synthesized waterborne polyurethane nanocomposites

$T_{d,max}$ (°C)	$T_{d,1/2}$ (°C)	$T_{d,onset}$ (°C)	POSS content (wt%)	Sample code
601	338	240	0.0	N_0
603	340	242	0.3	N_1
604	344	245	0.6	N_2
640	350	250	1.2	N_3
641	365	265	2.4	N_4
642	380	275	3.5	N_5
649	400	292	4.6	N_6

indicates the presence of the hard segments dispersion within the soft segments. The chain mobility of the soft segments is prevented by the restricted hard segments and this causes the T_g value of the soft microdomains to increase.

6. Thermogravimetric Analysis (TGA)

Fig. 6 depicts the thermal stability of the samples as a function of the POSS content. The initial decomposition temperature ($T_{d,onset}$), temperature of half decomposition ($T_{d,1/2}$), and temperature of the maximum decomposition ($T_{d,max}$) for different samples at a heating rate of 10 °C/min are shown in Table 5.

In Table 5, the initial decomposition temperature ($T_{d,onset}$) is the temperature at which the loss of weight during heating is measurable. The temperature of half decomposition ($T_{d,1/2}$) is the temperature at which the loss of weight reaches 50% and ($T_{d,max}$) denotes the maximum decomposition and means the temperature at which the loss of weight reaches its final value. This is observed through increasing the percentage of POSS; the thermal stability of the cast films is increased. There are two stages in the thermal degradation of aqueous polyurethanes; the first step is caused by the degradation of hard segments, and the second step is due to soft segment degradation [48,49]. Similarly, in this project, thermal degradation of the synthesized samples occurred in two steps. In the synthesis

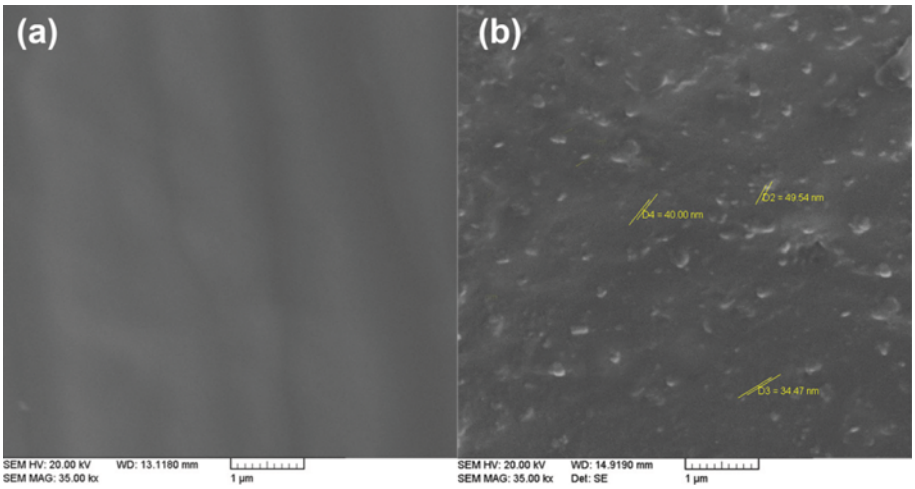

Fig. 7. SEM images of: (a) The neat PU and (b) nanocomposite based on 1.2 wt% POSS.

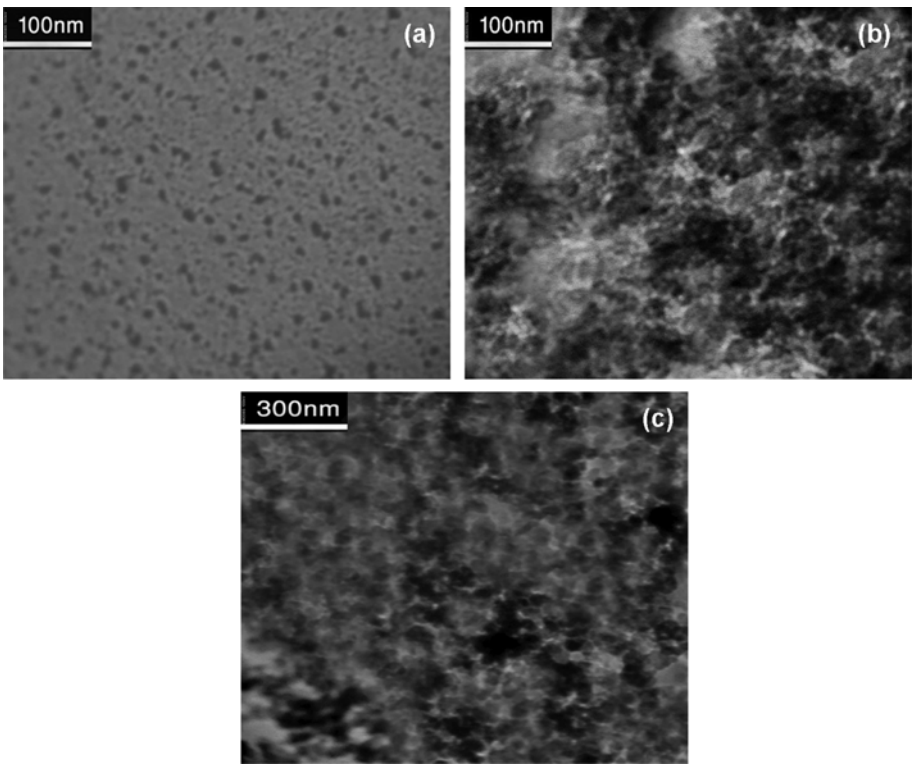

Fig. 8. TEM images of (a) the neat PU, (b) and (c) nanocomposite based on 1.2 wt% POSS at different magnifications.

route, POSS molecules were incorporated into the hard segments. Therefore, according to TGA data of pure POSS ($T_{d,onset}$=285, $T_{d,1/2}$=375 and $T_{d,max}$=699 °C), which was obtained in this research, with increasing the percentages of POSS, the thermal stability increased up to a maximum increase of more than 50 °C. The observed enhancement is due to a reduction in the mobility of hard segments in the presence of the bulky POSS pendant groups. With decreasing the mobility of the polymer chains, the crystallinity and, hence, the thermal stability were increased, which is in good agreement with results of similar in the literature [50,51].

7. Morphological Studies

It is important to understand whether POSS nanoparticles are dispersed homogeneously or not within the polyurethane backbone. The homogeneous dispersion of nanoparticles is necessary for obtaining high performance nanocomposites. Therefore, dispersion of the POSS particles in the matrix was investigated by SEM analysis. To give an example, SEM images of the fractured surfaces of the neat PU and the synthesized nanocomposite based on 1.2 wt% POSS taken at a magnification of 35000X are shown in Fig. 7.

Fig. 7(a) depicts the image of the neat PU and Fig. 7(b) the morphology of the nanocomposite containing 1.2 wt% POSS. In Fig. 7(b) the sample containing 1.2 wt% POSS shows homogeneous dispersion. Regarding this micrograph, one can clearly observe that complete dispersion of the POSS occurs in the sample with 1.2 wt% POSS.

To complete our morphological studies, the microphase separated morphology of the neat PU and the sample containing 1.2 wt% POSS was accurately evaluated by TEM measurement. Fig. 8 shows a comparison between TEM micrographs of the neat PU (Fig. 8(a)) and the sample including 1.2 wt% POSS at different magnifications (Figs. 8(b) and 8(c)).

In Fig. 8, the morphology of the sample containing 1.2 wt% POSS does not show any aggregation of POSS particles. This result indicates that POSS diol macromer has chemically reacted with hard segment and incorporated into the polymer matrix. Microphase-separated structure is detectable in two samples. It is clear that the sample with 1.2 wt% POSS shows a finer structure compared to that of the pure PU. In Figs. 8(a) and 8(b) the dark section represents the hard segments and the bright section represents the soft segments. In Fig. 8(b), it seems that with the incorporation of the POSS macromer into the polymer matrix the compatibility of the hard and the soft segments increases and the morphology is modified. The POSS nanoparticles have large surface area; therefore, a broad interaction zone with the PU segments is formed. This leads to a large volume fraction of the polymer matrix and better interaction with the nanoparticles [52]. Also, it seems that domain size in the sample including 1.2 wt% POSS decreased while miscibility increased. Decreasing the dimension of domain size by the incorporation of POSS nanoparticles into the other polymer matrices has been reported [53].

AFM measurements were made to evaluate the changes in the surface morphology. Three-dimensional AFM images displayed in Fig. 9 belong to the samples containing different amounts of POSS nanoparticles. The parameters of roughness were taken by analyzing scans of the topography image acquired from surface of the samples.

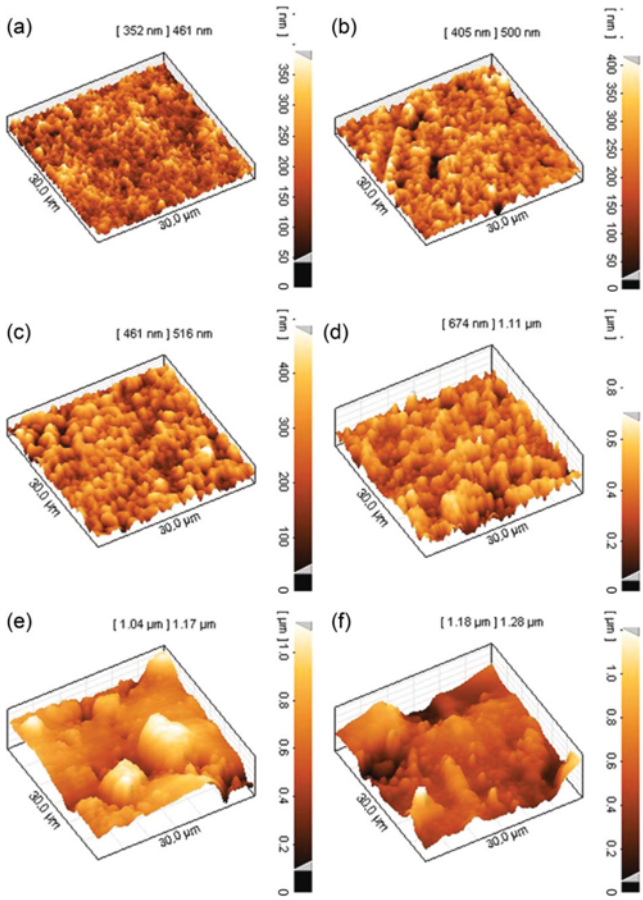

Fig. 9. Surface roughness of the samples as a function of POSS content: (a) 0.0 wt%, (b) 0.6 wt%, (c) 1.2 wt%, (d) 2.4 wt%, (e) 3.5 wt% and (f) 4.6 wt%.

Table 6. Surface roughness of the synthesized waterborne polyurethane nanocomposites

Sample code	POSS content (wt%)	S_a (nm)	S_q (nm)
a	0.0	47.0	58.4
b	0.6	62.4	78.9
c	1.2	65.5	82.3
d	2.4	90.0	110.0
e	3.5	122.0	160.0
f	4.6	132.0	171.0

Roughness parameters: including average roughness (S_a) and the root-mean-square (S_q) of the surfaces were determined using AFM images (Table 6) [54]. As can be seen in Fig. 9 and Table 6, with increasing of the POSS content in the samples, the surface roughness increased. The sample containing 4.6 wt% POSS showed the maximum value of the surface roughness.

Roughness enhancement with increased POSS content can be also seen in the 2D AFM phase images of the synthesized samples (Fig. 10). In Fig. 10 the incorporation of POSS in the soft segments increased with the POSS (white section) amount and microphase separation is reduced. Furthermore, the hard segments within the domains are oriented as a result of tangential deposition [55]. The

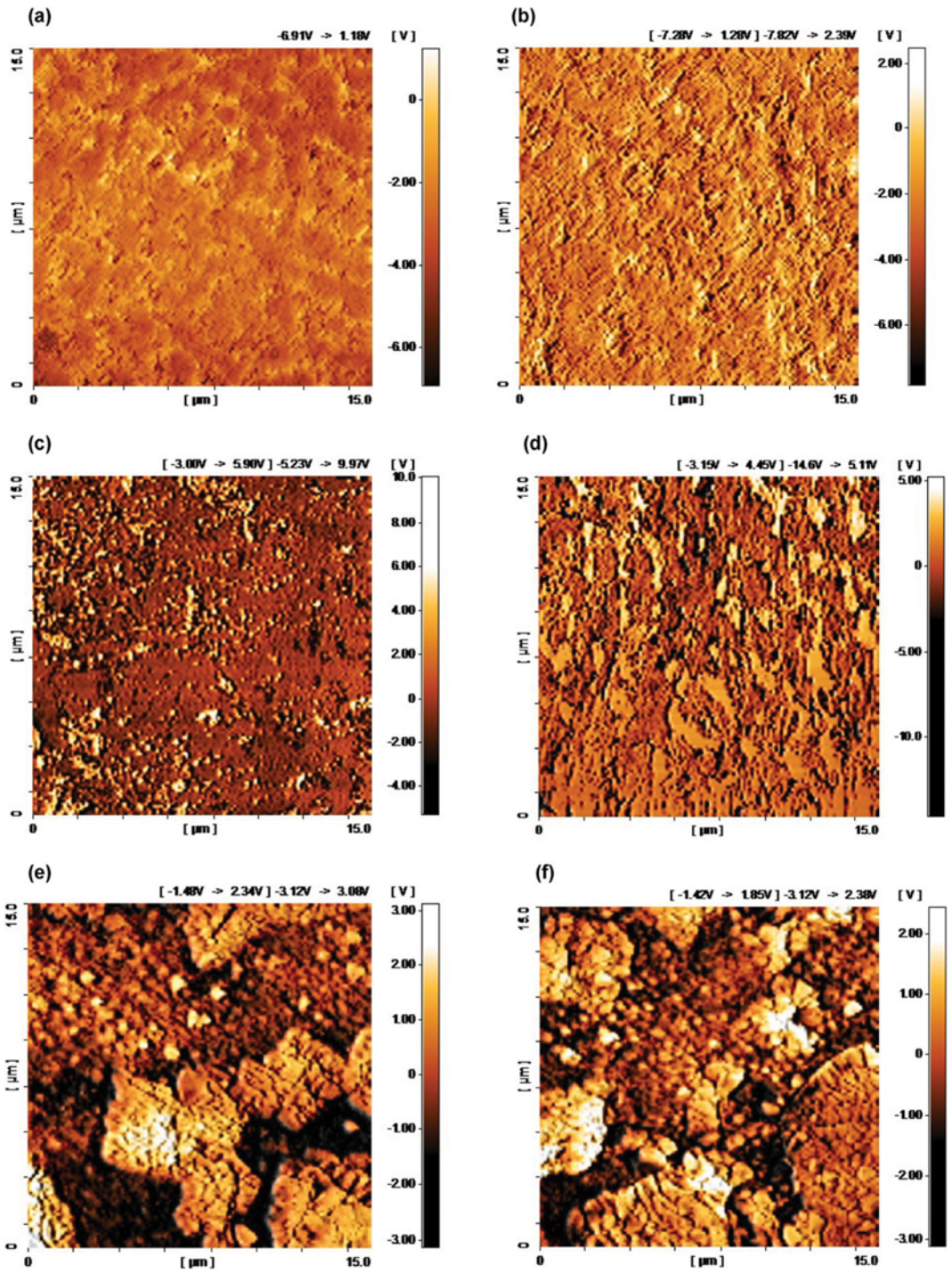

Fig. 10. 2D AFM phase images of the samples as a function of POSS content: (a) 0.0 wt%, (b) 0.6 wt%, (c) 1.2 wt%, (d) 2.4 wt%, (e) 3.5 wt% and (f) 4.6 wt%.

sample containing 1.2 wt% POSS (Fig. 10(c)) clearly has the optimum phase dispersion. In the samples containing higher amounts of POSS (2.4-4.6 wt%), POSS crystals are formed (Figs. 10(d)-10(f)). However, with further increase in POSS content, more POSS crystals are formed, which results in increased micro-phase segregation between POSS and the polymer phases. Concentration-dependent formation of POSS crystals within a polymer matrix has been previously reported [56].

CONCLUSIONS

A series of waterborne polyurethane nanocomposites were synthesized using different quantities of the reactive POSS nanoparticles up to a level of 4.6 wt%. Prepolymer mixing was performed for synthesis of the samples with 30 wt% solid content. All the compositions were stable for more than 10 months (no settling). The structure of the synthesized samples was studied by ATR-FTIR spec-

troscopy. Investigation of the functional groups supported the formation of PU-POSS nanocomposites. The results showed that particle size, viscosity, modulus, T_g, tensile strength, and thermal stability increased with the POSS contents. We used, BES sodium salt (as an internal ionic center) for the first time in synthesis of water-based polyurethane nanocomposites. Therefore, an additional step of neutralization was not necessary in our synthesis route. The X-ray diffraction studies revealed that the cages of POSS maintain a self assembling ability when incorporated to the hard segments of the polyurethane, and formed nanocrystalline phase. Morphological measurements demonstrated that incorporation of nanoparticles to the hard segments facilitated more compatibility and formation of a homogeneous structure. This conclusion was also confirmed by TEM analysis. Furthermore, AFM images showed that with increasing the POSS amounts, the surface roughness increased. The synthesized emulsions are promising candidates for applications as environment-friendly coatings.

REFERENCES

1. K. N. Raftopoulos and K. Pielichowski, *Prog. Polym. Sci.,* In Press (2015).
2. S. W. Kuo and F. C. Chang, *Prog. Polym. Sci.*, **36**, 1649 (2011).
3. D. B. Cordes, P. D. Lickiss and F. Rataboul, *Chem. Rev.*, **110**, 2081 (2010).
4. K. Pielichowski, J. Njuguna, B. Janowski and J. Pielichowski, *Adv. Polym. Sci.*, **201**, 225 (2006).
5. C. Sanchez, G. J. de A. A. Soler-Illia, F. Ribot, T. Lalot, C. R. Mayer and V. Cabuil, *Chem. Mater.*, **13**, 3061 (2001).
6. D. Neumann, M. Fisher, L. Tran and J. G. Matisons, *J. Am. Chem. Soc.*, **124**, 13998 (2002).
7. S. K. Yadav, S. S. Mahapatra, H. J. Ryu, H. J. Yoo and J. W. Cho, *React. Funct. Polym.*, **81**, 91 (2014).
8. A. Fina, D. Tabuani and G. Camino, *Eur. Polym. J.*, **46**, 14 (2010).
9. Y. Feng, Y. Jia, S. Guang and H. Xu, *J. Appl. Polym. Sci.*, **115**, 2212 (2010).
10. E. S. Cozza, O. Monticelli and E. Marsano, *Macromol. Mater. Eng.*, **295**, 791 (2010).
11. L. Ricco, S. Russo, O. Monticelli, A. Bordo and F. Bellucci, *Polymer*, **46**, 6810 (2005).
12. R. Misra, R. D. Cook and S. E. Morgan , *J. Appl. Polym. Sci.*, **115**, 2322 (2010).
13. P. Iyer, G. Iyer and M. Coleman, *J. Membr. Sci.*, **358**, 26 (2010).
14. Z. Zhang, G. Liang, J. Wang and P. Ren, *Polym. Compos.*, **28**, 175 (2007).
15. S. Y. Soong, R. E. Cohen and M. C. Boyce, *Polymer*, **48**, 1410 (2007).
16. E. T. Kopesky, G. H. McKinley and R. E. Cohen, *Polymer*, **47**, 299 (2006).
17. Y. Zhao and D. A. Schiraldi, *Polymer*, **46**, 11640 (2005).
18. H. Zhang, S. Kulkarni and S. L. Wunder, *J. Phys. Chem.* B., **111**, 3583 (2007).
19. Z. Wang, S. Leng, Z. Wang, G. Li and H. Yu, *Macromolecules*, **44**, 566 (2011).
20. Z. Wang, Z. Wang, H. Yu, L. Zhao and J. Qu, *RSC Adv.*, **2**, 2759 (2012).
21. Z. Zhou, N. Yin, Yo. Zhang and Yi. Zhang, *J. Appl. Polym. Sci.*, **107**, 825 (2008).
22. L. Song, S. Xuan, X. Wang and Y. Hu, *Thermochim. Acta*, **527**, 1 (2012).
23. L. Liu, Y. Hu, L. Song, X. Gu and Z. Ni, *Iran. Polym. J.*, **19**, 937 (2010).
24. R. Jeziorska, B. Swierz-Motysia, A. Szadkowska, B. Marciniec, H. Maciejewski, M. Dutkiewicz and I. Leszczynska, *Polimery*, **56**, 809 (2011).
25. E. Tegou, V. Bellas, E. Gogolides and P. Argitis, *Microelectron. Eng.*, **73-74**, 238 (2004).
26. M. Fiayyaz, K. M. Zia, M. Zuber, T. Jamil and M. K. Khosa, M. A. Jamal, *Korean J. Chem. Eng.*, **31**, 644 (2014).
27. M. Zuber, K. M. Zia, M. A. Iqbal, Z. T. Cheema, M. Ishaq and T. Jamil, *Korean J. Chem. Eng.*, **32**, 184 (2015).
28. Q. Zhang, X. Huang, X. Wang, X. Jia and K. Xi, *Polymer*, **55**, 1282 (2014).
29. D. Gnanasekaran and B. S. Reddy, *Polym. Int.*, **63**, 507 (2014).
30. J. P. Lewicki, K. Pielichowski, M. Jancia, E. Hebda, R. L. F. Albo and R. S. Maxwell, *Polym. Degrad. Stab.*, **104**, 50 (2014).
31. D. Przadka, J. Jeczalik, E. Andrzejewska, B. Marciniec, M. Dutkiewicz and M. Szlapka, *React. Funct. Polym.*, **73**, 114 (2013).
32. A. Solouk, M. Solati-Hashjin, S. Najarian, H. Mirzadeh and A. M. Seifalian, *Iran Polym. J.*, **20**, 91 (2011).
33. B. Janowski and K. Pielichowski, *Thermochim. Acta*, **478**, 51 (2008).
34. M. Barikani, H. Honarkar and Me. Barikani, *Monatsh. Chem.*, **141**, 653 (2010).
35. F. Mumtaz, M. Zuber, K. M. Zia, T. Jamil and R. Hussain, *Korean J. Chem. Eng.*, **30**, 2259 (2013).
36. M. Sultan, H. N. Bhatti, M. Zuber and M. Barikani, *Korean J. Chem. Eng.*, **30**, 488 (2013).
37. A. K. Nanda, D. A. Wicks, S. A. Madbouly and J. U. Otaigbe, *Macromolecules*, **39**, 7037 (2006).
38. S. Turri and M. Levi, *Mocromol. Rapid Commun.*, **26**, 1233 (2005).
39. X. Wang, Y. Hu, L. Song, W. Xing, H. Lu, P. Lv and G. Jie, *J. Polym. Res.*, **18**, 721 (2011).
40. K. Lewandowski, L. R. Krepski, D. E. Mickus, R. R. Roberts, S. M. Heilmann, W. K. Larson, M. D. Purgett, S. D. Koecher, S. A. Johnson, D. J. Mcgurran, C. J. Rueb, S. V. Pathre and K. A. M. Thakur, *J. Polym. Sci. Part A: Polym. Chem.*, **40**, 3037 (2002).
41. G. Socrates, *Infrared and raman characteristic group frequencies*, 3rd Ed., Wiley, London (2004).
42. H. T. Lee, S. Y. Wu and R. J. Jeng, *Colloids Surf., A: Physicochem. Eng. Aspects*, **276**, 176 (2006).
43. A. Barni and M. Levi, *J. Appl. Polym., Sci.*, **88**, 716 (2003).
44. B. X. Fu, W. Zhang, B. S. Hsiao, M. Rafailovich, J. Sokolov, G. Johansson, B. B. Sauer, S. Phillips and R. Balnski, *High Perform. Polym.*, **12**, 565 (2000).
45. C. Hepburn, *Polyurethane elastomers*, Applied Science, England (1982).
46. L. Zheng, R. J. Farris and E. B. Coughlin, *Macromolecules*, **34**, 8034 (2001).
47. H. Xu, S. W. Kuo, J. S. Lee and F. C. Chang, *Macromolecules*, **35**, 8788 (2002).
48. M. G. Lu, J. Y. Lee, M. J. Shim and S. W. Kim, *J. Appl. Polym. Sci.*, **85**, 2552 (2002).
49. N. Grassie and G. Scott, *Polymer degradation and stabilisation*, Cam-

bridge University, London (1985).
50. H. Liu and S. Zheng, *Macromol. Rapid Commun.*, **26**, 196 (2005).
51. S. Zhang, Q. Zou and L. Wu, *Macromol. Mater. Eng.*, **291**, 895 (2006).
52. Th. Kourkoutsaki, E. Logakis, I. Kroutilova, L. Matejka, J. Nedbal and P. Pissis, *J. Appl. Polym. Sci.*, **113**, 2569 (2009).
53. W. Zhang, B. X. Fu, Y. Seo, E. Schrag, B. Hsiao, P. T. Mather, N. L. Yang, D. Xu, H. Ade, M. Rafailovich and J. Sokolov, *Macromolecules*, **35**, 8029 (2002).
54. W. P. Dong, P. J. Sullivan and K. J. Stout, *Wear*, **178**, 29 (1994).
55. A. Aneja and G. L. Wilkes, *Polymer*, **44**, 7221 (2003).
56. V. N. Bliznyuk, T. A. Tereshchenko, M. A. Gumenna, Yu P. Gomza, A. V. Shevchuk, N. S. Klimenko and V. V. Shevchenko, *Polymer*, **49**, 2298 (2008).